Attenuating the ear canal feedback pressure of a laser-driven hearing aid

Morteza Khaleghi[a)]
Earlens Corporation, Menlo Park, California 94025, USA

Sunil Puria
Eaton-Peabody Laboratory, Massachusetts Eye and Ear Infirmary, Department of Otology and Laryngology, Harvard Medical School, 243 Charles Street, Boston, Massachusetts 02114, USA

(Received 5 September 2016; revised 6 January 2017; accepted 10 January 2017; published online 10 March 2017)

Microphone placement behind the pinna, which minimizes feedback but also reduces perception of the high-frequency pinna cues needed for sound localization, is one reason why hearing-aid users often complain of poor sound quality and difficulty understanding speech in noisy situations. In this paper, two strategies are investigated for minimizing the feedback pressure (thereby increasing the maximum stable gain, MSG) of a wide-bandwidth light-activated contact hearing aid (CHA) to facilitate microphone placement in the ear canal (EC): (1) changing the location of the drive force and its direction at the umbo, and (2) placing an acoustic damper within the EC to reduce the feedback pressure at the microphone location. The MSG and equivalent pressure output (EPO) are calculated in a 3D finite element model of a human middle ear based on micro computed tomography (micro-CT) images. The model calculations indicate that changing the umbo-force direction can decrease feedback pressure, but at the expense of decreased EPO. However the model shows improvements in MSG without sacrificing EPO when an acoustic damper is placed in the EC. This was verified through benchtop experimentation and in human cadaver temporal bones. The results pave the path towards a wide-bandwidth hearing aid that incorporates an EC-microphone design. © *2017 Acoustical Society of America*.
[http://dx.doi.org/10.1121/1.4976083]

[CAS] Pages: 1683–1693

I. INTRODUCTION

Two shortcomings that hearing-aid users often complain about include poor sound quality and difficulty comprehending speech in noisy environments (Turner and Henry, 2002; Kochkin, 2010). These issues can be understood in terms of the limitations of acoustic hearing aids to restore audibility above 4–5 kHz, due to a sharp roll-off in their output above ~5 kHz, which is related to the amount of energy needed to move the diaphragm of the speaker and the relative inefficiency of air coupling at high frequencies (Valente, 2002; Aazh *et al.*, 2012). The limited bandwidth of conventional hearing aids not only reduces perceived sound quality, but also limits the possibility of amplifying the high-frequency pinna-diffraction cues that are needed to localize sound sources and thereby improve understanding of speech in noisy environments (Noble *et al.*, 1997; Moore *et al.*, 2010; Levy *et al.*, 2015). However, even if a hearing aid were able to faithfully amplify high-frequency sounds, it would still need to have its microphone located near the entrance of the ear canal (EC) in order for the pinna-diffraction cues to be picked up in the first place. This poses a significant design challenge due to the amount of acoustic feedback that the microphone would be susceptible to at this location with a non-occluded EC.

To overcome the bandwidth limitations of typical acoustic hearing aids, a contact hearing aid (CHA) has been designed and built to allow subjects to hear amplified sounds from 0.125 to 10 kHz (Fay *et al.*, 2013; Puria *et al.*, 2016; Gantz *et al.*, 2017). The Earlens CHA operates under the hypothesis that restoring hearing across an extended frequency range can provide the human brain with the information it needs to understand speech in complex and noisy environments. The CHA works differently from an acoustic hearing aid that produces amplified acoustic energy into the EC; instead, as shown in Fig. 1(a), the CHA mechanically drives (i.e., vibrates) the umbo directly via a customized umbo platform that is placed in contact with the center of the tympanic membrane (TM). The CHA consists of three main subsystems: the Processor; the custom-made Light Tip, which houses an infrared laser emitter; and the Tympanic Lens, which mechanically drives the umbo. The Processor receives and processes environmental sound captured by a microphone and converts it into a pulse-density modulation (PDM) signal, which is then used to drive the near-infrared laser source (with a central wavelength of 830 nm and a nominal power of 5 mW) located within the Light Tip. The Tympanic Lens in the CHA [Fig. 1(b)] is held in place by a ring-shaped perimeter platform customized to fit along the skin near the outer edge of the TM, and consists of a photodetector, a tiny balanced-armature microactuator, and a thin umbo platform that gently contacts the center of the TM. The photodetector receives the light signal from the Light

[a)]Electronic mail: khaleghi29@gmail.com

FIG. 1. (Color online) The Earlens CHA: (a) current design of the CHA, which consists of a Processor with a microphone, a vented Light Tip placed in the EC that transforms digital signals into pulses of laser light, and a Tympanic Lens that uses the power and signal encoded in the light beam to mechanically drive the umbo; and (b) an enlarged view of the Tympanic Lens with custom-made Perimeter and Umbo Platforms.

Tip and converts it into an electrical current that then activates the microactuator, causing it to vibrate the TM at the umbo. Both Light Tip and Tympanic Lens are custom-made components that are designed and manufactured uniquely for each patient based on their own EC and TM geometries.

By coupling the microactuator directly to the umbo, the Tympanic Lens is much more effective than an acoustic device at providing gain above 5 kHz (Fay *et al.*, 2013; Puria *et al.*, 2016; Gantz *et al.*, 2017). In this manner, the CHA should have the sound-quality advantages of an implantable device (Kiefer *et al.*, 2006), but with the further advantages of being non-surgical and easily removable (see Puria, 2013, for a review).

However, in spite of the bandwidth advantages and relative efficiency of the CHA, placement of its microphone at the entrance of the EC in order to fully capture high-frequency pinna-diffraction cues may still be limited by acoustic feedback. Acoustic feedback in hearing aids refers to the acoustical coupling between the speaker and the microphone of the hearing aid (Agnew, 1996; Puria, 2003), which limits the maximum gain that the hearing aid can provide before the feedback causes instability, i.e., the maximum stable gain (MSG). Although the CHA does not use a speaker to directly inject sound into the EC, which would pose an obvious feedback problem for a microphone located at the entrance of the EC, the fact that it mechanically vibrates the umbo means that the TM surface also ends up moving, and this in turn generates a moderate amount of feedback pressure that can reduce the MSG of the system as it travels laterally through the EC and is picked up by the microphone.

The goals of this research are to (1) characterize the EC feedback pressure (ECFP) due to umbo-drive forces; (2) characterize the MSG and equivalent pressure output (EPO) of the Earlens CHA system by measuring the sound- and umbo-driven stapes velocity and the ECFP; and (3) investigate potential methods for increasing the MSG of the system while minimally affecting the EPO, using a three-dimensional (3D) finite element (FE) model, benchtop experiments, and measurements on human temporal bones (TBs), in order to facilitate future microphone placement at the entrance of the EC.

II. METHODS

In order to improve the MSG of the system, the feedback pressure due to mechanical stimulation of the umbo (i.e., the ECFP) should be reduced. In this paper, different techniques for mitigating the ECFP are first investigated numerically using an FE model, and then the most promising techniques are tested experimentally using both benchtop and human temporal bone (TB) measurements.

A. FE modeling

A multiphysics FE model of the human ear has been developed in COMSOL Multiphysics (version 5.1), based on the acoustics–solid interaction between the air in the EC and the TM, which in turn sets the ossicular chain into vibration. The model is based on a reconstructed 3D geometry obtained from micro computed tomography (micro-CT) data, and has been validated against experimental measurements (Cai *et al.*, 2010; O'Connor *et al.*, 2016). The model includes the most medial 1 cm-long section of the EC that is terminated with an impedance boundary condition of $\rho^*c = 418$ kg/(s.m^2), representing air at 25 °C. The acoustic field of the EC is coupled with the solid-mechanics physics of the rest of the middle- and inner-ear structures, including the TM, tympanic annulus, malleus, incus, stapes, incudomalleolar joint (IMJ), incudostapedial joint (ISJ), stapes annular ligament, and suspensory ligaments. The cochlear load is modeled as a massless impedance boundary condition (Merchant *et al.*, 1996; Aibara *et al.*, 2001).

In the case of acoustic stimulation, a plane acoustic wave with an appropriate frequency and magnitude of 1 Pa is introduced at the entrance of the EC. For mechanical stimulation (i.e., the case of CHA drive), a harmonic force boundary condition is introduced along the malleus and at the umbo in specified directions, with a flat magnitude of 0.8 mN, which causes the TM and middle ear to vibrate. In

both acoustic and mechanical excitation cases, 50 logarithmically spaced frequencies from 0.1 to 12 kHz are used to stimulate the middle ear.

B. Measurements and data analysis

To experimentally characterize the effect of dampers on the magnitude of the ECFP, a benchtop measuring system was developed. As shown in Fig. 2(a), it contains a silicone replica of the human outer ear, which is based on the right ear of a 62-year-old male subject. A sound source representing the TM-generated feedback pressure is placed at the medial end of the EC, at the center of where the TM would be. Pressure measurements are then made using two probe-tube microphones, respectively located on the medial and lateral sides of the Light Tip.

In addition to the benchtop measurements, and as shown in Figs. 2(b) and 2(c), the ECFP and MSG of the system are characterized using temporal bone measurements. All of the TBs are purchased from Innoved Institute (Rosemont, IL). To provide a realistic impedance boundary condition at the lateral end of the EC, all of the TBs have an intact pinna [e.g., Fig. 2(b)]. A Tympanic Lens and Light Tip are custom-made for each TB, based on the geometrical dimensions of the TM and EC.

To determine the ECFP and MSG of each temporal bone, measurements of EC pressure ($\boldsymbol{P}_{EC}$) and stapes velocity ($\boldsymbol{V}_{ST}$) are acquired in response to EC sound pressure and due to mechanical stimulation of the umbo over a sweep of 230 logarithmically spaced frequencies from 0.1 to 12 kHz. The middle ear cavity and in particular, the stapes are accessed by drilling out the mastoid and opening the facial recess (Aibara *et al.*, 2001; Sudhoff *et al.*, 2011). The stimulus voltage provided by the measurement system drives a simplified Processor circuit in order to drive the Light Tip and Tympanic Lens during the measurements. $\boldsymbol{P}_{EC}$ is measured at the EC entrance (and in one case within 3 mm of the TM as well) using an ER-7 C probe-tube microphone (Etymotic Research, Elk Grove Village, IL), and $\boldsymbol{V}_{ST}$ is measured using a Polytec HLV-1000 Laser Doppler Vibrometer (LDV; Polytec, Irvine, CA).

All measurements are made using a custom LabVIEW-based synchronous-averaging measurement software called SyncAv (Gottlieb *et al.*, 2016). In the present experiments, an NI USB-4431 data-acquisition module (National Instruments, Austin, TX) with a maximum sampling rate of 96 kHz was used. The sampling rate, Fast Fourier Transform (FFT) length, and number of averages were 48 kHz, 4096, and 10, respectively.

From the measurements of $\boldsymbol{V}_{ST}$ and $\boldsymbol{P}_{EC}$, the following quantities are calculated:

- The baseline sound-driven stapes transfer function without the Tympanic Lens on the TM. This is computed by dividing the sound-driven stapes velocity, $\boldsymbol{V}_{ST}$, by the driving sound pressure in the EC at a location within 3 mm of the TM, $\boldsymbol{P}_{EC}$, and can be written as $(\boldsymbol{V}_{ST}/\boldsymbol{P}_{EC})|_{\text{Sound}}$. In temporal-bone (TB) experiments, the driving sound pressure is equalized to be 1 Pa across the frequency range (using the Stimulus Equalization feature of SyncAv).
- The EPO of the system. This is computed by dividing the light-driven stapes velocity, $\boldsymbol{V}_{ST}|_{\text{Light}}$, by the baseline sound-driven transfer function, such that $\mathbf{EPO} = \boldsymbol{V}_{ST}|_{\text{Light}} / (\boldsymbol{V}_{ST}/\boldsymbol{P}_{EC})|_{\text{Sound}}$.
- The MSG of the system. This is computed by, first, taking the ratio of $\boldsymbol{V}_{ST}|_{\text{Light}}$ and the light-driven feedback pressure, $\boldsymbol{P}_{EC}|_{\text{Light}}$, i.e., $(\boldsymbol{V}_{ST}/\boldsymbol{P}_{EC})|_{\text{Light}}$, and then dividing that ratio by the baseline sound-driven transfer function, such that $\mathbf{MSG} = (\boldsymbol{V}_{ST}/\boldsymbol{P}_{EC})|_{\text{Light}} / (\boldsymbol{V}_{ST}/\boldsymbol{P}_{EC})|_{\text{Sound}}$.

III. RESULTS

A. FE model results

Two different strategies for improving of the system's efficacy are first tested in the FE model to predict their effects on the MSG and EPO: (1) changes at the source of the feedback pressure (i.e., changes to the stimulation scenarios of the umbo), and (2) attenuation of the acoustic feedback pressure as it travels laterally from the TM to the EC entrance.

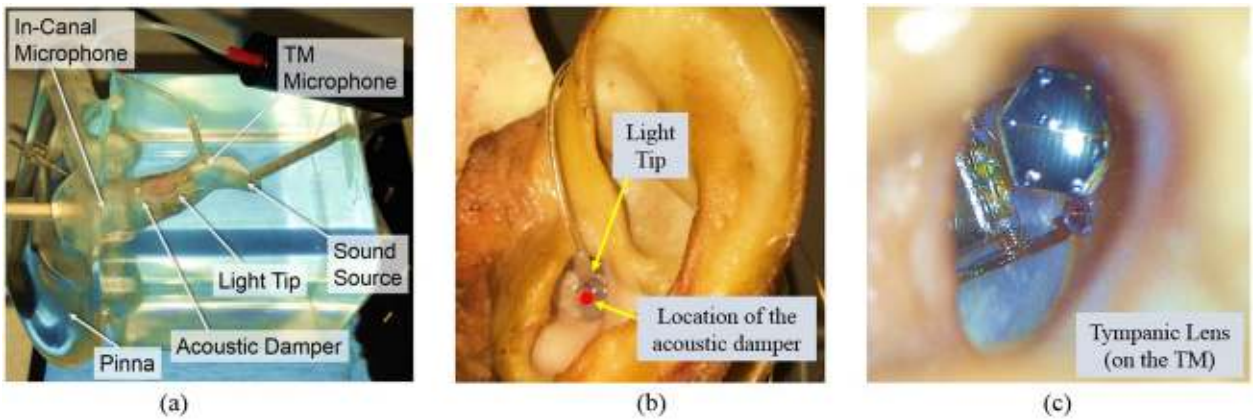

FIG. 2. (Color online) Experimental setups for characterizing the ECFP: (a) benchtop measurement setup using a silicone replica of a human external ear, including the pinna and EC, with a sound source at the most medial end of the EC to simulate ECFP generated by the TM, and a microphone on each side of the Light Tip to measure changes in ECFP along the EC feedback path; (b) TBs with intact pinnae are used in the measurements to include proper pinna cues when measuring the ECFP; and (c) a close-up image of the Tympanic Lens after placement on the TM.

1. FE model calculations of the baseline MSG and EPO

First, the MSG and EPO are calculated for the baseline FE-model response to umbo stimulation, which corresponds to the normal working behavior of the Tympanic Lens. In this case, the umbo of the TM is mechanically driven along an axis perpendicular to the plane of the tympanic ring, and there are no external components or changes made to the acoustic feedback path from the TM to the entrance of the EC. Figure 3 shows the baseline MSG and EPO, as obtained by the baseline 3D FE model (solid line) and as obtained with the Earlens system in experimental tests using four TBs (dashed lines, from Puria *et al.*, 2016). The main difference between the FE model and experimental setup is that, in the model, the force delivered to the umbo is a constant-amplitude harmonic force that pushes on a rigid reference frame, whereas in the CHA, the bias springs attached to the chassis [shown in Fig. 1(b)] act as a non-rigid support for the force generated by the microactuator. This difference only affects the low-frequency stimuli (below 800 Hz), since at higher frequencies the mass of the microactuator dominates the response and the force applied to the umbo can be very well approximated by a constant-amplitude harmonic force.

As shown in Fig. 3(a), the MSG of the system features a broad minimum of about 15 dB in the 1–4 kHz mid-frequency region, when the microphone is placed in close proximity to the TM (3 mm lateral to the TM, per Puria *et al.*, 2016). As the frequency decreases below 1 kHz and increases above 4 kHz, the MSG improves and can be greater than 40 dB above 6 kHz. The high MSG magnitudes at low frequencies can be described by, first, considering the low magnitudes of the corresponding baseline sound-driven transfer function in the denominator of the MSG calculations, and, second, the fact that the corresponding feedback pressure wavelengths are long (greater than 35 cm) and the generated feedback pressure can easily escape the EC. On the other hand, the high MSG magnitudes at higher frequencies can be understood by recalling the out-of-phase vibrational patterns of the TM under high-frequency stimulation, in which the sound pressure generated by each location of the TM gets cancelled, or attenuated, by the pressure generated by other neighboring locations (Puria, 2003; Rosowski *et al.*, 2013; Khaleghi *et al.*, 2016). The MSG at low and high frequencies is adequate to treat a large number of patients. However, at mid frequencies the MSG is lower and can result in feedback, when the microphone is placed in the EC. It should be noted that moving the microphone laterally towards the EC entrance will improve the MSG; however, this improvement is not sufficient to treat patients that have significant hearing loss in the mid-frequency region (Moore and Sek, 2013). For this reason the MSG, particularly in the mid-frequency region, needs to be improved, and it is desirable to do this without feedback cancellers since they produce undesirable distortions to speech (Chi *et al.*, 2003; Maxwell and Zurek, 1995).

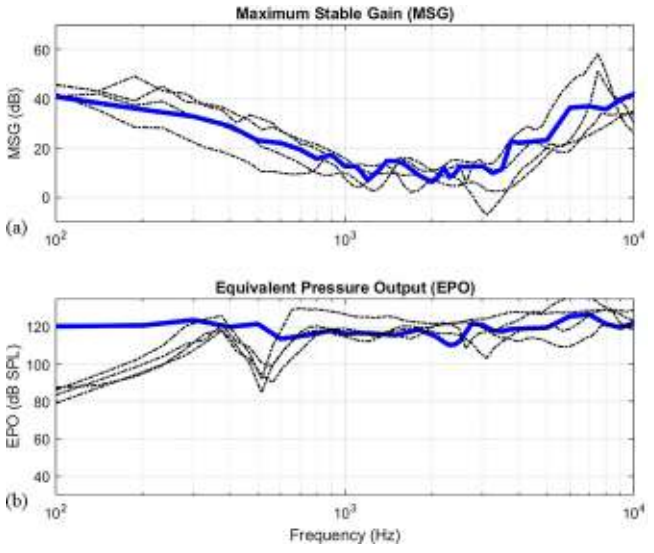

FIG. 3. (Color online) Comparison of the results obtained with the 3D FE model (solid lines) and those obtained from four TB measurements (dashed lines): (a) MSG; and (b) EPO.

The close agreement between the EPO in the measurements and model, of approximately 120 dB sound pressure level (SPL) from 0.8 to 12 kHz [Fig. 3(b)], indicates that the microactuator mass impedance is greater than the umbo impedance, such that the body of the microactuator stays relatively fixed, which leads to a constant force from the armature (the vibrating element of the microactuator) to the umbo. Below 0.8 kHz, the modeled and measured EPO diverge and differ by up to 40 dB at 0.1 kHz. In addition, there is a dip in the measured EPO of up to 20–35 dB in the 0.4–0.6 kHz range that is not predicted in the FE results. These differences are primarily due to the lower inertial impedance, of the CHA relative to the umbo impedance, and due to the non-rigid supporting feature of the bias springs, which together result in non-constant-amplitude harmonic force from the microactuator to the umbo in the experiments.

With the baseline MSG and EPO characterized, several possible scenarios for improving the MSG by performing some modifications to the 3D FE model of the middle ear are investigated. The design-change scenarios include changing the location of the force vector along the malleus and changing the direction of the force vector at the umbo, and also placing an acoustic damper in the EC to attenuate the TM-generated feedback pressure before being picked up by the microphone. More-efficient approaches will be those with higher MSG across frequencies, but with negligible negative effects on the EPO.

2. Changing the direction of the umbo force vector in the FE model

As described earlier, unlike conventional hearing aids that use a speaker to drive the middle ear, the CHA directly vibrates the umbo with a custom-made umbo platform that is connected to a balanced-armature transducer via a drive post [Fig. 1(b)]. Therefore, the direction of the force vector that drives the middle ear (through the umbo) could play an important role in the output of the system. In the FE model, the force vector is defined as a 3D boundary load applied at the umbo. As shown in Fig. 4, the x–y plane is considered to be the plane of the tympanic ring, and the z-axis is the axis perpendicular to this plane, pointing towards the medial direction. In the current design, the nominal angle between

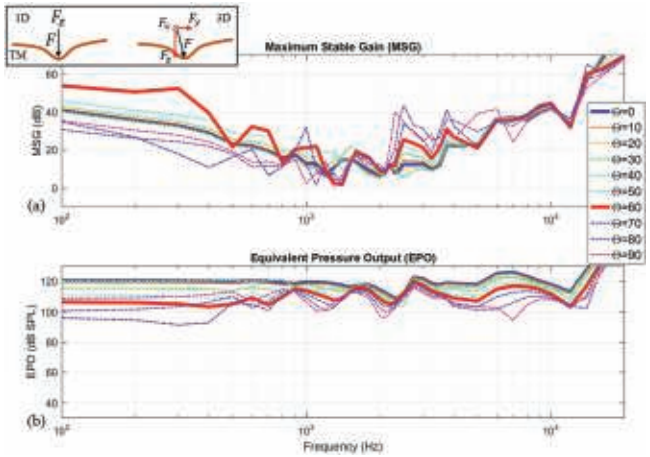

FIG. 4. Effects of the direction of the umbo force vector on the (a) MSG; and (b) EPO, for the 1D force vector (thick solid blue lines, corresponding to $\theta = 0°$) and various 3D force vectors (thick solid red lines for the $\theta = 60°$ case, along with thin dash-dotted lines for other θ angles). The magnitude of the force vector in all cases is equal to 0.8 mN and the direction of the force vectors is varied from the normal direction ($\theta = 0°$) in the 1D case to 90° from the normal direction ($\theta = 90°$) in the 3D cases.

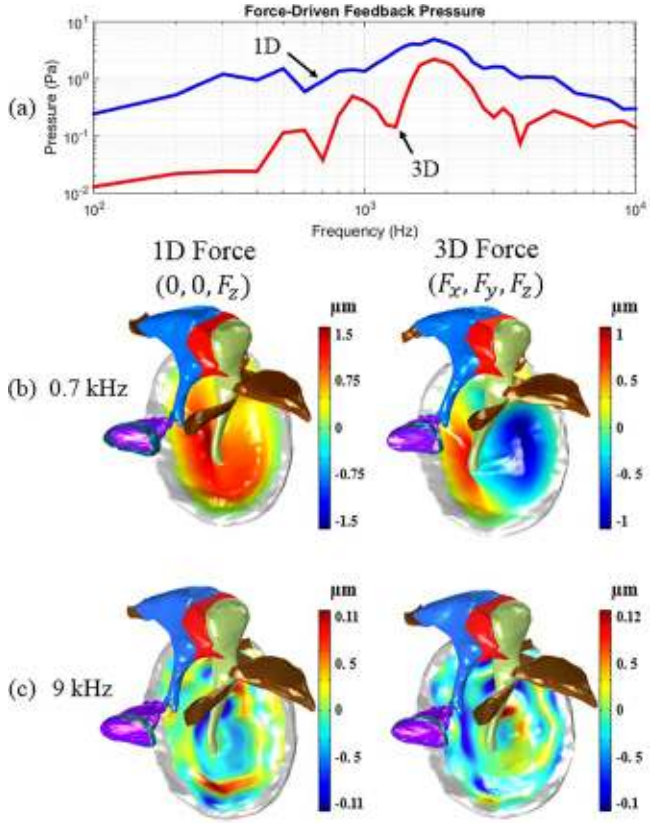

FIG. 5. (Color online) Umbo-driven feedback pressure and TM vibration patterns in the FE model: (a) ECFP magnitudes for the 1D case ($\theta = 0°$ in Fig. 4) and an example 3D case ($\theta = 60°$ in Fig. 4). Corresponding vibrational patterns of the TM surface at (b) 0.7 kHz and (c) 9 kHz for the 1D (left) and 3D (right) umbo force cases. The significantly lower ECFP of the 3D case at 0.7 kHz corresponds to distinctly out-of-phase motion of the anterior and posterior halves of the TM, as compared to the largely in-phase motion of the TM in the 1D case that produces a higher ECFP. The similar degree of complexity in the TM modes for the two force directions at 9 kHz corresponds to a reduced gap between the two ECFP values.

the force vector and the plane of the tympanic ring is 90°. Therefore, it can be labeled "1D", which is a force vector with its x and y components set to 0.

To understand the effects of varying the direction of the umbo force vector on the MSG and EPO, the x, y, and z components of the force vector are varied in the model with its magnitude kept constant. As shown in Fig. 4, the component angles of the force vectors are adjusted in the FE model to simulate equal-amplitude force vectors with directions varying from 0° (i.e., the 1D case with a direction perpendicular to the plane of the tympanic ring) up to 90° from the nominal case (i.e., parallel to the plane of the tympanic ring). The 1D case (shown with solid blue lines) and a representative 3D case (shown with solid red lines) are highlighted in Fig. 4 for comparison purposes. Although some loading scenarios provide higher MSG at certain frequencies, still the 1D force vector with the x and y force components set to zero ($\theta = 0°$) is considered to be the most efficient one, as it generally provides the highest EPO across all the frequencies.

It is also important to understand how the direction of the umbo force vector affects the resulting feedback pressure. Figure 5 compares the EC feedback pressure generated by the 1D and 3D force vectors corresponding to the two labeled thick solid blue and red lines in Fig. 4, respectively. As shown in Fig. 5(a), for all of the frequency points, the magnitude of the ECFP is smaller for the 3D case in comparison to the 1D case. As an example, at 0.7 kHz, the feedback pressure in the 3D case is almost 25 dB smaller than in the 1D case. The cause of this difference can be further understood if one looks at the vibrational patterns of the TM, which essentially acts like a loudspeaker and is the source of the feedback pressure. Figures 5(b) and 5(c) compare the vibrational patterns of the TM at two example frequency points of 0.7 and 9 kHz. As shown in Fig. 5(b), at 0.7 kHz, all the points on the surface of the TM vibrate almost in phase in the case of the 1D force, whereas in the corresponding 3D case there is almost a 180° phase difference between the anterior and posterior halves of the TM, which causes the feedback pressure on the two sides to essentially cancel out and therefore significantly reduce the overall EC feedback pressure. As the excitation frequency increases, the complexity of the vibrational patterns of the TM continues to increase (Tonndorf and Khanna, 1972; Rosowski *et al.*, 2009; Khaleghi *et al.*, 2015). For instance, as shown in Fig. 5(c), at 9 kHz, the vibrational patterns of the TM in both the 1D case and an example 3D case ($\theta = 60°$) are similarly complex; therefore, as shown in Fig. 5(a), the generated ECFPs in the two cases are closer to each other at this frequency.

3. Changing the location of the mechanical force stimulation along the malleus

It has been hypothesized that better sound-transmission efficiency might be possible through stimulation of the short process of the malleus rather than the umbo (Paulick *et al.*, 2014). To test this hypothesis, the MSG and EPO are calculated for a force applied at the short process of the malleus. As before, the magnitudes of the force vectors are both equal

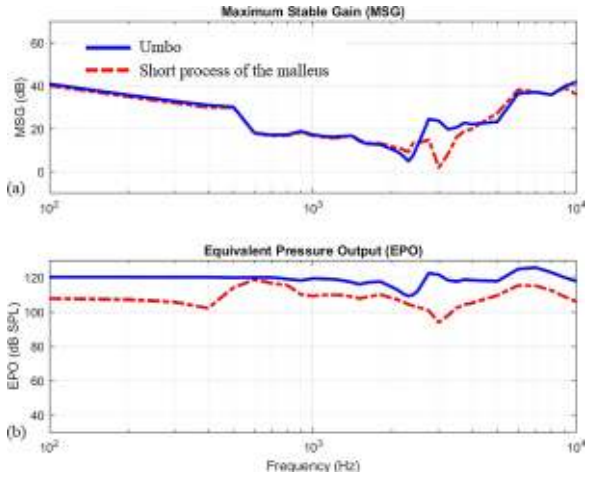

FIG. 6. (Color online) The effect on (a) MSG and (b) EPO of changing the location of the force vector from the umbo to the short process of the malleus. The magnitude of the force vectors in both cases is 0.8 mN, and the directions are both perpendicular to the plane of the tympanic ring. The MSG in both cases is almost equal, whereas the EPO decreases, by as much as 25 dB, when the force is applied to the short process of the malleus.

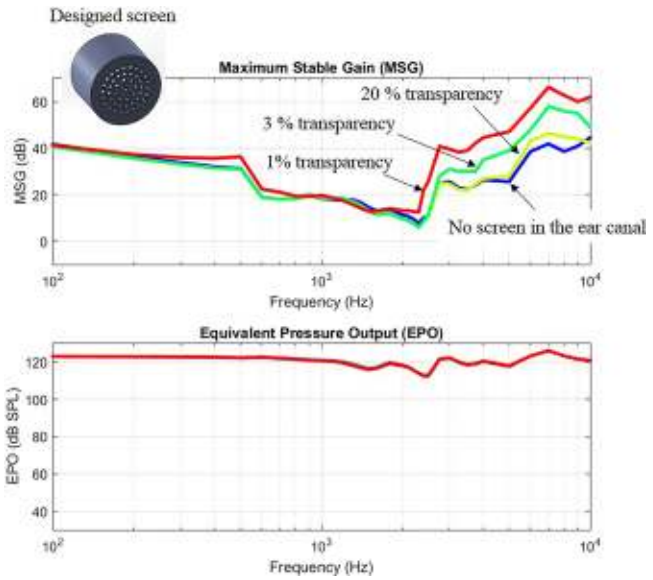

FIG. 7. (Color online) FE investigations of placing an acoustic absorber (inset image) within the EC show improvements in MSG (top), while having a negligible effect on the EPO (bottom). The transparency percentage is the ratio of the total area occupied by the holes in the screen over the total cross-sectional area of the screen, which is the area of a circle with a diameter of 6 mm.

to 0.8 mN. As shown in Fig. 6, across most of the frequency points, the MSG is similar for the two locations. However, stimulating the short process of the malleus instead of the umbo leads to reduction in the EPO that ranges from about 2 dB at 0.6 kHz to as much as 25 dB at 3 kHz. This can be further explained by recalling the ossicular chain lever action (Wever *et al.*, 1948), which states that the force between the TM and the oval window increases by approximately 2.3 dB due to a lever-like mechanism between the malleus and the incus, with different lengths ($L_{\text{malleus}}/L_{\text{incus}} = 1.3$), undergoing a relative rotational motion around the pivotal point (fulcrum). As the loading location moves to the short process of the malleus, the effective length of the malleus decreases, thereby decreasing the effective force at the oval window. The effective force direction is potentially another contributing factor for reducing the EPO to values lower than what is expected from the lever ratio, so that when the force is applied to the short process of the malleus, the most efficient direction is not necessarily the same as for the umbo. Thus, this result contradicts the hypothesis and indicates that changing the force location from the umbo to the short process of the malleus is not an effective way of improving the EPO of the system.

4. Modeling the effects of an acoustic screen in the EC

As described in the previous two sections, changes to the loading conditions (i.e., changing the direction or location of the drive force) may help to improve the MSG, but at the undesirable cost of decreasing the EPO. Another potential design change to test with the FE model is the addition of a resistive acoustic screen to the feedback path (i.e., within the EC) in order to attenuate the EC feedback pressure. As shown in the inset image of Fig. 7, a cylindrical screen with an outer diameter of 6 mm and a mesh diameter of 200 μm is placed in the EC at a distance of 10 mm from the TM. It should be noted that commercially available acoustic dampers (or screens) have fine mesh dimensions ($<30\,\mu$m), which makes their FE modeling challenging and computationally expensive; however, the goal of this simplified model is to study the feasibility of improving the MSG using these screens without affecting the EPO. The number of the holes (mesh density) of the screen is varied to represent different resistance values of the damper. For simplicity, a transparency ratio (expressed as a percentage) is defined as the ratio of the total area of the holes in the screen to the total area of the screen (i.e., 9π mm^2). As shown in Fig. 7, the results illustrate promising improvements in the MSG above 2 kHz, while minimally affecting the EPO. However, this approach needs to be experimentally tested.

B. Benchtop and TB experiments

Based on the numerical investigations, the promising approach of placing an acoustic screen (damper) in the EC is experimentally tested to see whether the feedback pressure can be reduced, thus improving the MSG, while having a negligible effect on the system's EPO. Two sets of experimental tests are performed: benchtop measurements and experiments on TBs.

1. Benchtop measurements using a silicone replica of a human external ear to characterize the attenuation of ear canal feedback pressure (ECFP)

To characterize the effects of (1) spatial separation between the source of ECFP and the microphone, and (2) a damper placed in the acoustic path of the ECFP, we developed a benchtop experimental setup with a silicone replica of the human EC and pinna [as shown in Fig. 2(a)]. The

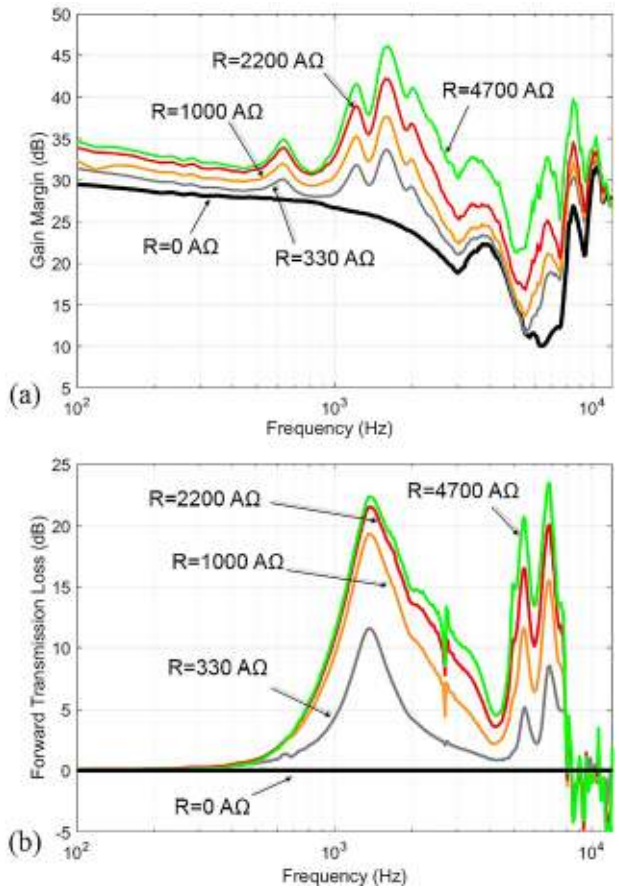

FIG. 8. (Color online) Characterization of backward and forward pressure attenuations across an acoustic damper in the EC, obtained using a silicone benchtop replica of a human external ear: (a) the backward gain margin measurements are obtained by comparing the pressure near the TM to the pressure at the EC entrance, when the sound source is at the TM. The bottommost line (R = 0 AΩ) shows the gain margin with no acoustic damper in the Light Tip. The other lines show how the gain margin increases as the resistor value of the damper in the Light Tip's vent hole increases in value from 330 to 4700 AΩ; and (b) the forward transmission loss indicates the attenuation of environmental sound on its way to the TM due to the presence of the same range of acoustic dampers in the Light Tip. This is obtained by comparing the pressure at the EC entrance to the pressure near the TM when the sound source is a free-field loudspeaker.

results, shown in Fig. 8, illustrate the improvement in the gain margin of the system when an acoustic damper, with a resistance value (R) expressed in acoustic ohms (AΩ), is placed in the vent hole of the EC Light Tip. In Fig. 8(a), the backward gain margin is calculated by taking the dB difference between the sound pressure level measured medial to the damper in the Light Tip and that measured lateral to the damper in the Light Tip (i.e., the ratio of the pressure (in Pa) measured by the microphone closest to the "TM" sound source over the pressure measured by the microphone placed at the entrance to the EC). The bottommost line shows the characteristic gain of the system without the use of a damper in the Light Tip (R = 0 AΩ), which is mostly due to the geometry-induced resonances of the EC as well as the distance between the two microphone locations, and also due to the reduction in pressure at the EC entrance as the closed space of the EC opens up to the air. The baseline gain margin (R = 0 AΩ) is 30 dB at 0.1 kHz and decreases with increasing frequency, reaching a minimum of about 10 dB in the 6–7 kHz region. Above 8 kHz, it rises back up to about 30 dB. These frequency-dependent effects are primarily due to the EC radiation impedance at low frequencies and the resonances of the EC and Light Tip geometries at mid and high frequencies (Hammershøi and Møller, 1996; Rosowski *et al.*, 1988). Placing dampers in the vent hole of the Light Tip (R ≥ 330 AΩ) generally increases the gain margin further as the resistor value increases. Using the most resistive damper in the Light Tip (R = 4700 AΩ), the maximum improvement in the gain margin, due to ECFP attenuation by the damper, reaches as high as 20 dB.

Figure 8(b) shows the sound attenuation in the forward direction (i.e., for sound traveling from the outside environment toward the TM). Placing a damper in the Light Tip attenuates sound transmission by less than 2 dB for frequencies below 0.7 kHz, independent of the R value, and increases to nearly 22 dB around 1.4 kHz for R = 4700 AΩ. The forward transmission loss reduces to less than 5 dB at frequencies around 4 kHz and raises back to about 20 dB for R = 4700 AΩ around 6–7 kHz. The forward transmission loss above 8 kHz is negligible. The one caveat about these benchtop measurements is that the absorption of sound by a natural TM and middle ear, which represent some damping characteristics, will result in reduced magnitudes of the peaks and valleys present in the forward transmission loss curve [Fig. 8(b)] (Zhang and Gan, 2010; Motallebzadeh *et al.*, 2013; Motallebzadeh *et al.*, 2016). Furthermore, it is worth noting that the shapes of the gain margins shown in Fig. 8(a) are different than the MSG calculations from the FE model shown in Fig. 7(a). The MSG results predicted by the FE model indicate increasing gain above 2 kHz as the damping increases (i.e., as the transparency of the screen decreases), but very little change below 2 kHz. This corresponds to a low-pass filter acting on the ECFP. In the benchtop experimental measurements, on the other hand, the effects of the damper are more complex across the frequency range. The main reason for this difference is that in the FE model, a simplified rigid geometry with relatively coarse mesh dimensions (200 μm) for the dampers are considered, whereas the dampers used in the experiments have finer mesh dimensions (<30 μm) and are made out of flexible woven filter cloth. In addition, unlike the dampers used in the experiments, the simplified damper in the FE model has a mesh depth of 1 mm, which acts not only as a resistive element but also as an acoustic mass element that introduces low-pass filter characteristics.

2. Baseline sound-driven stapes velocity in temporal bones

After characterizing the acoustic effects of a damper in the EC using a silicone replica of the human outer ear, the dampers are next tested on three human TB specimens. The experimental procedure for acquiring and processing the data have been described in Sec. II. It should be noted that the $(\boldsymbol{V}_{ST}/\boldsymbol{P}_{EC})|_{\text{Sound}}$ transfer function was determined by recording $\boldsymbol{V}_{ST}$ in response to a sound-pressure stimulus that was equalized at each frequency to produce a constant pressure value of 1 Pa at a microphone location close to the TM.

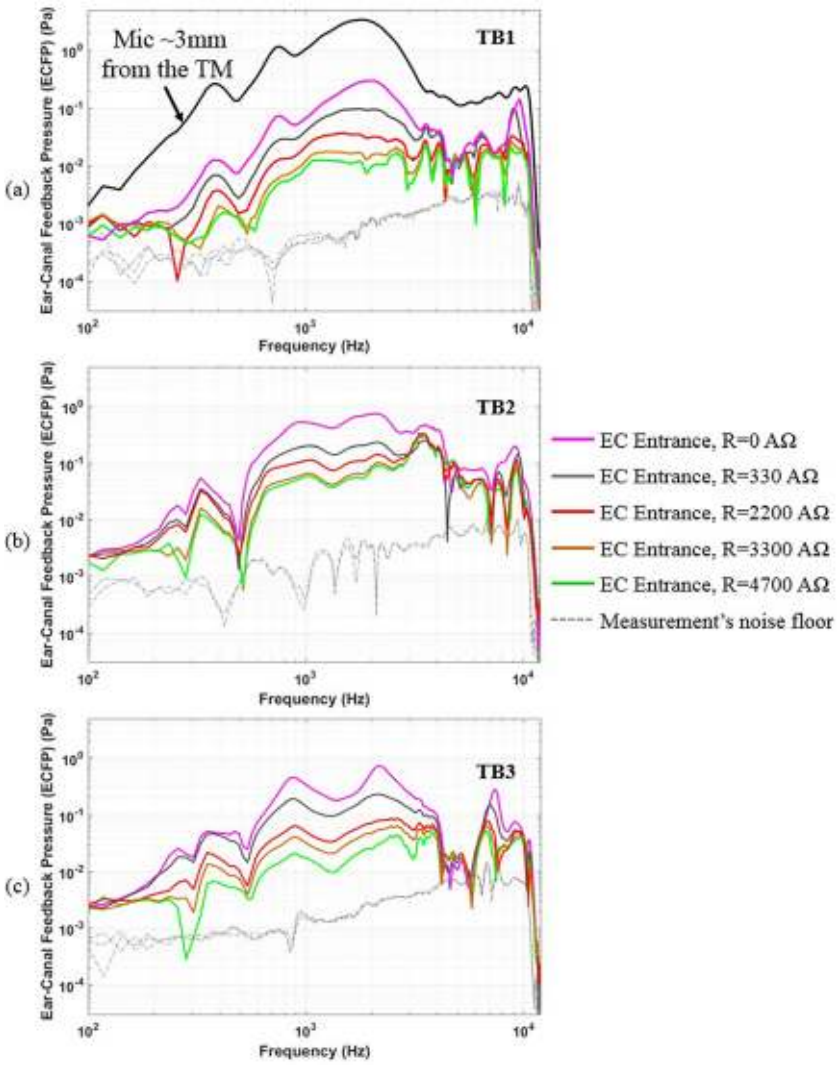

FIG. 9. (Color online) Experimental characterization of the ECFP on three TBs [TB1, TB2, and TB3 are shown in (a), (b), and (c), respectively], measured at the EC entrance for a range of acoustic-damper resistance values within the Light Tip vent, including the case with just an open vent (magenta lines). For TB1 (a), the pressure is also measured at a medial location approximately 3 mm from the TM (black line) to show how the ECFP is attenuated by moving the microphone laterally to the entrance of the EC (magenta line). The dashed gray lines show the noise floor of the measurements.

This was accomplished using the Stimulus Equalization function in the SyncAv measurement software, which is able to apply a different gain at each stimulus frequency when driving the speaker, such that a uniform sound-pressure amplitude is presented at the microphone location across all frequencies. In addition, the V_{ST} measurements are compared to the ASTM standard F2504 for TB models, to ensure that the TB responses are within the normal and acceptable range (Rosowski *et al.*, 2007).

3. TB measurements of the ECFP

Figure 9 shows the ECFP measurements in three TBs with and without the use of an acoustic damper in the Light Tip. In this figure, the magenta lines represent the baseline ECFP across the entire frequency range, as measured by a microphone located at the entrance of the EC, without any damper in the Light Tip (R = 0 AΩ). For each TB, four additional Light Tips, one for each of four acoustic resistance values (R = 330, 2200, 3300, and 4700 AΩ), were manufactured with the resistive screen placed at the lateral opening of the vent, and the ECFP is then measured using each Light Tip in turn. In TB1, the ECFP is also measured at a location approximately 3 mm from the TM, accomplished by inserting the microphone probe tube through the open vent of the Light Tip, so as to characterize the effects on the measured ECFP of increasing the separation between the microphone and the feedback source (i.e., the TM vibration). As shown in Fig. 9(a), by moving the microphone from a point 3 mm from the TM (uppermost line) to the EC entrance (magenta line, R = 0 AΩ), the ECFP decreases at a rate of approximately 1 dB/mm for much of the frequency range (given the 20 mm distance between the two microphone locations). Figure 9 also indicates that, for all three TBs [Fig. 9(a)–9(c)], the highest attenuations in the ECFP due to the acoustic damper occur between 0.4 and 4 kHz, which is an ideal frequency range for improving the MSG with a damper, since this is where it normally has its lowest values (based on the baseline MSG data shown in Fig. 3).

4. Improvements in the MSG using an acoustic damper within the EC

Figure 10 shows a variety of MSG measurements for the CHA, as measured on TB1. With the microphone at the EC entrance and without a damper in the Light Tip (R = 0 AΩ;

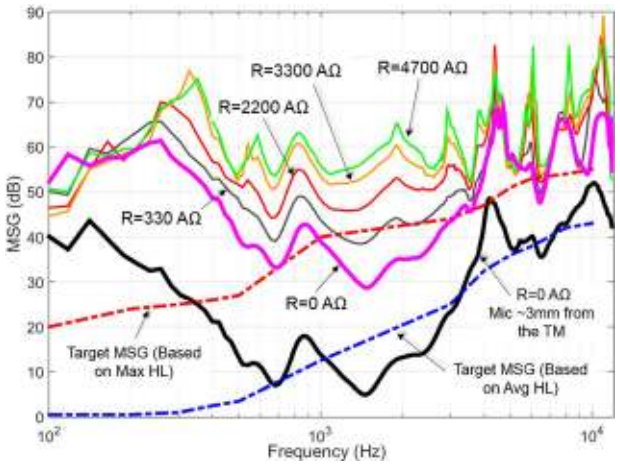

FIG. 10. (Color online) Characterization of the MSG of the system for TB1, using ECFP measurements at two locations (~3 mm from the TM in one case and at the EC entrance otherwise), and using a damper in the Light Tip with different acoustic resistances. Target MSGs are also shown for fitting subjects who have the maximum hearing loss (red dashed line) and for fitting subjects with average hearing loss (blue dashed line) (Fay *et al.*, 2013), based on the CAM2 fitting algorithm (Moore and Sek, 2013).

magenta line), the MSG is typically at least 15–20 dB higher than the MSG with the microphone located approximately 3 mm from the TM. With the microphone at the EC entrance, the MSG for the R = 0 AΩ case decreases from about 60 to 40 dB as the frequency increases from 0.1 to 1 kHz, and exhibits a broad minimum of about 30 dB in the 1–4 kHz range. Above this frequency range, the MSG rises back up to about 50–60 dB. The MSG is also shown for the Light Tips with different acoustic dampers placed within the lateral vent opening (R = 330, 2200, 3300, and 4700 AΩ), as well as the target gains required for subjects with average (blue dashed line) and maximum (red dashed line) hearing losses, based on the CAM2 fitting algorithm (Moore and Sek, 2013; Levy *et al.*, 2015). Compared to the target MSGs, it is clear that this particular TB could even exceed the target MSG based on the maximum hearing loss (red dashed line) with a Light Tip damper value of greater than 330 AΩ. Measurements on the other two TBs exhibit similar MSG improvements for the different damper values, suggesting that the majority of subjects can be fit with a Mic-in-Canal CHA if an appropriate damper is placed in their Light Tips' vent hole. However, the baseline MSG varies across the TBs, as is to be expected.

IV. DISCUSSION

Unlike conventional acoustic hearing aids, the CHA does not use a speaker for the delivery of amplified sound. Instead, it mechanically drives the umbo to transduce amplified sound to the middle and inner ears. The driven umbo also produces vibrations of the eardrum that acts as a loudspeaker that generates sound. But the eardrum vibrations break up into modes, particularly at the higher frequencies, and thus the radiated sound partially cancels itself, resulting in lower pressure in the EC (Puria, 2003). This is why the MSG of the CHA can be significantly higher than that of conventional acoustic hearing aids. The Earlens CHA is unique in that MSGs of more than 50 dB can be achieved at low and high frequencies with an open EC and without the use of feedback-cancellation algorithms. While feedback-cancellation algorithms can be used with the CHA to further reduce feedback in the mid frequency range where the MSG is at its lowest (from 1 to 4 kHz), the focus of this study has been to investigate purely acousto-mechanical techniques for improving the MSG of devices that mechanically stimulate the middle ear.

A. Attenuation of the ECFP at the source

It has been shown through holographic techniques that the TM exhibits complex vibrational patterns under transient or harmonic excitations, in which different points on the surface of the TM vibrate in- or out-of-phase with respect to one another (Tonndorf and Khanna, 1972; Rosowski *et al.*, 2013; Khaleghi *et al.*, 2016). Thus, the total feedback pressure that passes into the EC will be the result of the overall volume displacements of air caused by these complex multiphasic motions. If all the points on the TM surface were to vibrate in phase with one another, then the maximum (i.e., the worst) feedback pressure would be produced, and conversely, if half the points on the TM surface were to vibrate completely out-of-phase with the other half (assuming equal areas and magnitudes), then the total volume displacement would be close to zero and theoretically no net feedback pressure would be produced. The vibrational patterns of the TM are affected by the boundary conditions, material properties, and loading condition of the TM. While the boundary conditions and material properties cannot be changed in intact ears, the loading condition can potentially be modified in order to reduce the TM-generated feedback pressure. Two potential strategies for improvement of the MSG were numerically tested, the first of which was to vary the direction of the mechanical force, and the second of which was to change the location of the applied force. The FE results show that changing the loading condition (umbo force direction) may improve the MSG at some frequency points [Fig. 4(a)]. However, this comes at the cost of decreasing the EPO of the system [Fig. 4(b)], which therefore makes it an unfavorable option for the CHA. Changing the location of the umbo force from the umbo to the short process of the malleus resulted in a decrease in output [Fig. 6(b)], as expected from a lever-mechanism point of view.

B. Attenuation of the ECFP using an acoustic damper

The unique sound-transduction mechanism of the CHA, involving direct mechanical stimulation of the umbo, enables the use of acoustic dampers in the EC to attenuate the feedback pressure without affecting the EPO of the system. Furthermore, compared with conventional hearing aids, in which the source of the feedback is the speaker of the hearing aid, the CHA's feedback source is the vibration of the TM, which can be thought of as an inefficient loudspeaker that provides significantly lower feedback pressure than a hearing-aid loudspeaker. The CHA's normally high MSG above about 4 kHz (Fig. 3), combined with the observed improvements in the mid-frequency MSG in the temporal bone experiments due to placing an acoustic damper in the

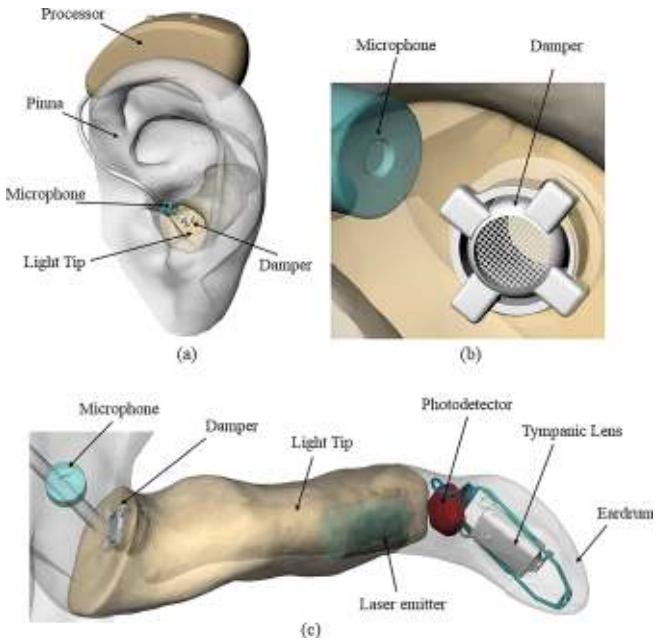

FIG. 11. (Color online) Placement of the acoustic damper within the Light Tip to improve the MSG of the system and allow microphone placement inside the EC: (a) a transparent view of the pinna showing the location of the Processor, in-canal microphone, damper, and the Light Tip; (b) a close-up view of the in-canal microphone and the damper placed in the lateral side of the Light Tip; and (c) a detailed view of the EC and the Earlens CHA showing how the laser-driven Tympanic Lens sits on the eardrum and the TM-generated feedback pressure gets attenuated by the damper before being picked up by the microphone.

Light Tip (Fig. 10), led to the hypothesis that a system combining a CHA with a damper would achieve high enough MSGs to adequately fit nearly all subjects with a microphone at the EC entrance, including subjects with the most severe hearing loss in the CHA fitting criteria. Measurements of the CHA in TBs (N = 3) with a variety of damper values (Fig. 10) show that it is possible to place a microphone near the EC entrance while providing the required gains in the 0.1 to 12 kHz range.

C. Where to place the acoustic damper?

Two main requirements should be considered when choosing an appropriate location for the damper within the Light Tip. First, given that these acoustic dampers are vulnerable to cerumen (i.e., ear wax), they should be placed in an area with the least possible risk of being clogged. Considering epithelial migration, which causes cerumen to move gradually from the medial to the lateral side of the EC, and given the proximity of the TM to the medial side of the Light Tip, placement of the damper on the lateral side of the Light Tip is preferred to avoid contact with cerumen. Second, the effects of damper placement on acoustic performance were measured experimentally by alternately placing the damper on the medial and lateral sides of the Light Tip, and the results show that placing the damper on the lateral side of the Light Tip attenuates the ECFP by almost 2 dB more than when it is placed on the medial side of the Light Tip (not shown).

On the basis of this study, Fig. 11 shows a proposed new CHA design with the damper placed on the lateral side of the Light Tip. Pinna localization cues are captured by the in-canal microphone and transmitted (with some attenuation) through the damper to the eardrum. This allows the user to experience a partially open environment. The damper attenuates the TM-generated feedback pressure before being picked by the in-canal microphone. Any occlusion effects due to the damper are yet to be determined and will be the subject of future experiments.

V. SUMMARY AND CONCLUSIONS

There are many potential benefits of a hearing device with a microphone placed in the EC that can pick up acoustic cues from the pinna. The use of acoustic cues above 5 kHz results in improved sound localization, spatial awareness, and auditory scene representation for normal-hearing listeners. Therefore, providing these benefits to hearing-impaired listeners may lead to an improved ability to hear in noisy situations, which would address one of the major complaints of current hearing-aid users. While the acoustic feedback pressure generated by hearing devices that mechanically stimulate the umbo tends to be significantly lower than that of acoustic hearing aids with a vented EC, it can still be too high for patients with severe hearing losses in the mid frequency range, which limits the placement of a microphone in the EC for these patients. In this study, numerical and experimental approaches were investigated for reducing the ECFP generated by one such device, the Earlens CHA. The results indicate that attempting to reduce the ECFP by altering the umbo-force vector does increase the MSG, but this is not a viable option because it also reduces the output, as measured by the EPO. However, both numerical and experimental results do suggest that placement of an acoustic damper within the EC (i.e., within the vent of the CHA's Light Tip) can reduce the ECFP at the EC entrance, while minimally affecting the EPO of the system, which paves the way toward placement of the microphone in the EC for future devices that mechanically stimulate the middle ear.

ACKNOWLEDGMENTS

The authors would like to thank Kevin N. O'Connor for providing editorial assistance.

Aazh, H., Moore, B. C., and Prasher, D. (**2012**). "The accuracy of matching target insertion gains with open-fit hearing aids," Am. J. Audiol. **21**(2), 175–180.
Agnew, J. (**1996**). "Acoustic feedback and other audible artifacts in hearing aids," Trends Amplif. **1**(2), 45.
Aibara, R., Welsh, J. T., Puria, S., and Goode, R. L. (**2001**). "Human middle-ear sound transfer function and cochlear input impedance," Hear. Res. **152**(1), 100–109.
Cai, H., Jackson, R. P., Steele, C., and Puria, S. (**2010**). "A biological gear in the human middle ear," in *Proceedings of COMSOL*, Vol. 28, p. 46.
Chi, H. F., Gao, S. X., Soli, S. D., and Alwan, A. (**2003**). "Band-limited feedback cancellation with a modified filtered-X LMS algorithm for hearing aids," Speech Commun. **39**(1), 147–161.
Fay, J. P., Perkins, R., Levy, S. C., Nilsson, M., and Puria, S. (**2013**). "Preliminary evaluation of a light based contact hearing device for the hearing impaired," Otol. Neurotol. **34**(5), 912.
Gantz, B. J., Perkins, R., Murray, M., Levy, S. C., and Puria, S. (**2017**). "Light-driven contact hearing aid for broad-spectrum amplification: safety and effectiveness pivotal study," Otol. Neurotol. **38**(3), 352–359.

Gottlieb, P. K., Li, X., Monfared, A., Blevins, N., and Puria, S. (**2016**). "First results of a novel adjustable-length ossicular reconstruction prosthesis in temporal bones," Laryngoscope **126**, 2559–2564.
Hammershøi, D., and Møller, H. (**1996**). "Sound transmission to and within the human ear canal," J. Acoust. Soc. Am. **100**(1), 408–427.
Khaleghi, M., Cheng, J. T., Furlong, C., and Rosowski, J. J. (**2016**). "In-plane and out-of-plane motions of the human tympanic membrane," J. Acoust. Soc. Am. **139**(1), 104–117.
Khaleghi, M., Guignard, J., Furlong, C., and Rosowski, J. J. (**2015**). "Simultaneous full-field 3-D vibrometry of the human eardrum using spatial-bandwidth multiplexed holography," J. Biomed. Opt. **20**(11), 111202–111202.
Kiefer, J., Arnold, W., and Staudenmaier, R. (**2006**). "Round window stimulation with an implantable hearing aid (Soundbridge®) combined with autogenous reconstruction of the auricle–a new approach," ORL **68**(6), 378–385.
Kochkin, S. (**2010**). "MarkeTrak VIII: Consumer satisfaction with hearing aids is slowly increasing," Hear. J. **63**(1), 19–20.
Levy, S. C., Freed, D. J., Nilsson, M., Moore, B. C., and Puria, S. (**2015**). "Extended high-frequency bandwidth improves speech reception in the presence of spatially separated masking speech," Ear Hear. **36**(5), e214–e224.
Maxwell, J. A., and Zurek, P. M. (**1995**). "Reducing acoustic feedback in hearing aids," IEEE Trans. Speech Audio Process. **3**(4), 304–313.
Merchant, S. N., Ravicz, M. E., and Rosowski, J. J. (**1996**). "Acoustic input impedance of the stapes and cochlea in human temporal bones," Hear. Res. **97**(1), 30–45.
Moore, B. C., Füllgrabe, C., and Stone, M. A. (**2010**). "Effect of spatial separation, extended bandwidth, and compression speed on intelligibility in a competing-speech task," J. Acoust. Soc. Am. **128**(1), 360–371.
Moore, B. C., and Sek, A. (**2013**). "Comparison of the CAM2 and NAL-NL2 hearing aid fitting methods," Ear Hear. **34**(1), 83–95.
Motallebzadeh, H., Charlebois, M., and Funnell, W. R. J. (**2013**). "A nonlinear viscoelastic model for the tympanic membrane," J. Acoust. Soc. Am. **134**(6), 4427–4434.
Motallebzadeh, H., Maftoon, N., Pitaro, J., Funnell, W. R. J., and Daniel, S. J. (**2016**). "Finite-element modelling of the acoustic input admittance of the newborn ear canal and middle ear," J. Assoc. Res. Otol. **18**, 25–48.
Noble, W., Byrne, D., and Ter-Horst, K. (**1997**). "Auditory localization, detection of spatial separateness, and speech hearing in noise by hearing impaired listeners," J. Acoust. Soc. Am. **102**(4), 2343–2352.
O'Connor, K. N., Cai, H., Gottlieb, P., Steel, C. R., and Puria S. (**2016**). "Varying the material properties of the human ossicular chain in a 3D finite-element model to examine their effects on middle-ear sound transmission," in *The International Union of Theoretical and Applied Mechanics - Symposium on Advances in Biomechanics of Hearing* (Stuttgart, Germany).
Paulick, P. E., Merlo, M. W., Mahboubi, H., Djalilian, H. R., and Bachman, M. (**2014**). "A micro-drive hearing aid: A novel non-invasive hearing prosthesis actuator," Biomed. Microdev. **16**(6), 915–925.
Puria, S. (**2003**). "Measurements of human middle ear forward and reverse acoustics: Implications for otoacoustic emissions," J. Acoust. Soc. Am. **113**(5), 2773–2789.
Puria, S. (**2013**). "Middle ear hearing devices," in *The Middle Ear* (Springer, New York), pp. 273–308.
Puria, S., Santa Maria, P. L., and Perkins, R. (**2016**). "Temporal-bone measurements of the maximum equivalent pressure output and maximum stable gain of a light-driven hearing system that mechanically stimulates the umbo," Otol. Neurotol. **37**(2), 160–166.
Rosowski, J. J., Carney, L. H., and Peake, W. T. (**1988**). "The radiation impedance of the external ear of cat: Measurements and applications," J. Acoust. Soc. Am. **84**(5), 1695–1708.
Rosowski, J. J., Chien, W., Ravicz, M. E., and Merchant, S. N. (**2007**). "Testing a method for quantifying the output of implantable middle ear hearing devices," Audiol. Neurotol. **12**(4), 265–276.
Rosowski, J. J., Cheng, J. T., Ravicz, M. E., Hulli, N., Hernandez-Montes, M., Harrington, E., and Furlong, C. (**2009**). "Computer-assisted time-averaged holograms of the motion of the surface of the mammalian tympanic membrane with sound stimuli of 0.4–25 kHz," Hear. Res. **253**(1), 83–96.
Rosowski, J. J., Dobrev, I., Khaleghi, M., Lu, W., Cheng, J. T., Harrington, E., and Furlong, C. (**2013**). "Measurements of three-dimensional shape and sound-induced motion of the chinchilla tympanic membrane," Hear. Res. **301**, 44–52.
Sudhoff, H., Dazert, S., and Hagen, R. (**2011**). "Basic surgery of the temporal bone," in *Manual of Temporal Bone Exercises* (Springer, Berlin, Germany), pp. 5–29.
Tonndorf, J., and Khanna, S. M. (**1972**). "Tympanic-membrane vibrations in human cadaver ears studied by time-averaged holography," J. Acoust. Soc. Am. **52**(4B), 1221–1233.
Turner, C. W., and Henry, B. A. (**2002**). "Benefits of amplification for speech recognition in background noise," J. Acoust. Soc. Am. **112**(4), 1675–1680.
Valente, M. ed. (**2002**). *Hearing Aids: Standards, Options, and Limitations* (Thieme, New York), Vol. 2.
Wever, E. G., Lawrence, M., and Smith, K. R. (**1948**). "The middle ear in sound conduction," Archiv. Otolaryngol. **48**(1), 19–35.
Zhang, X., and Gan, R. Z. (**2010**). "Dynamic properties of human tympanic membrane-experimental measurement and modelling analysis," Int. J. Exp. Comput. Biomech. **1**(3), 252–270.